JGR Atmospheres

RESEARCH ARTICLE
10.1029/2018JD029726

Arctic Amplification Response to Individual Climate Drivers

Camilla Weum Stjern[1], Marianne Tronstad Lund[1], Bjørn Hallvard Samset[1], Gunnar Myhre[1], Piers M. Forster[2], Timothy Andrews[3], Olivier Boucher[4], Gregory Faluvegi[5,6], Dagmar Fläschner[7], Trond Iversen[8], Matthew Kasoar[9], Viatcheslav Kharin[10], Alf Kirkevåg[8], Jean-François Lamarque[11], Dirk Olivié[8], Thomas Richardson[2], Maria Sand[1], Dilshad Shawki[9], Drew Shindell[12], Christopher J. Smith[2], Toshihiko Takemura[13], and Apostolos Voulgarakis[9]

[1]CICERO Center for International Climate and Environmental Research, Oslo, Norway, [2]University of Leeds, Leeds, UK, [3]Met Office Hadley Centre, Exeter, UK, [4]Institut Pierre-Simon Laplace, Université Pierre et Marie Curie/CNRS, Paris, France, [5]Center for Climate Systems Research, Columbia University, New York, NY, USA, [6]NASA Goddard Institute for Space Studies, New York, NY, USA, [7]Max Planck Institute for Meteorology, Hamburg, Germany, [8]Norwegian Meteorological Institute, Oslo, Norway, [9]Imperial College London, London, UK, [10]Canadian Centre for Climate Modelling and Analysis, Victoria, British Columbia, Canada, [11]NCAR/UCAR, Boulder, CO, USA, [12]Nicholas School of the Environment, Duke University, Durham, NC, USA, [13]Kyushu University, Fukuoka, Japan

Abstract The Arctic is experiencing rapid climate change in response to changes in greenhouse gases, aerosols, and other climate drivers. Emission changes in general, as well as geographical shifts in emissions and transport pathways of short-lived climate forcers, make it necessary to understand the influence of each climate driver on the Arctic. In the Precipitation Driver Response Model Intercomparison Project, 10 global climate models perturbed five different climate drivers separately (CO_2, CH_4, the solar constant, black carbon, and SO_4). We show that the annual mean Arctic amplification (defined as the ratio between Arctic and the global mean temperature change) at the surface is similar between climate drivers, ranging from 1.9 ($\pm$ an intermodel standard deviation of 0.4) for the solar to 2.3 ($\pm$0.6) for the SO_4 perturbations, with minimum amplification in the summer for all drivers. The vertical and seasonal temperature response patterns indicate that the Arctic is warmed through similar mechanisms for all climate drivers except black carbon. For all drivers, the precipitation change per degree global temperature change is positive in the Arctic, with a seasonality following that of the Arctic amplification. We find indications that SO_4 perturbations produce a slightly stronger precipitation response than the other drivers, particularly compared to CO_2.

Key Points:
- Arctic amplification of surface warming is similar between global drivers of climate change
- Black carbon induces differing vertical and seasonal amplification patterns
- Sulfate affects Arctic precipitation responses more strongly than other drivers, particularly in the summer season

Supporting Information:
- Supporting Information S1

Correspondence to:
C. W. Stjern,
camilla.stjern@cicero.uio.no

Citation:
Stjern, C. W., Lund, M. T., Samset, B. H., Myhre, G., Forster, P. M., Andrews, T., et al. (2019). Arctic amplification response to individual climate drivers. *Journal of Geophysical Research: Atmospheres*, *124*, 6698–6717. https://doi.org/10.1029/2018JD029726

Received 26 SEP 2018
Accepted 23 MAY 2019
Accepted article online 10 JUN 2019
Published online 2 JUL 2019

Author Contributions:
Conceptualization: Marianne Tronstad Lund
Data curation: Bjørn Hallvard Samset, Timothy Andrews, Olivier Boucher, Gregory Faluvegi, Dagmar Fläschner, Trond Iversen, Matthew Kasoar, Viatcheslav Kharin, Alf Kirkevåg, Jean-François Lamarque, Dirk Olivié, Thomas Richardson, Dilshad Shawki, Drew Shindell, Christopher J. Smith, Toshihiko Takemura, Apostolos Voulgarakis
Writing – review & editing: Marianne Tronstad Lund, Bjørn Hallvard Samset, Piers M. Forster, Timothy Andrews, Olivier Boucher, *(continued)*

1. Introduction

Both observations and climate models indicate that the temperature increase in the Arctic has been substantially larger than the globally averaged warming since preindustrial times (Cowtan & Way, 2014; Hartmann et al., 2013; Holland & Bitz, 2003). This phenomenon is known as Arctic amplification (AA). Locally, the AA involves pronounced reductions in sea ice cover (AMAP, 2017; Kay et al., 2011; Notz & Stroeve, 2016), increasing Arctic methane emissions from permafrost degradation (Anthony et al., 2016), changes to the mass balance of glaciers and ice sheets (Shepherd et al., 2012), and detrimental influences on Arctic ecosystems (Hinzman et al., 2013) and indigenous peoples (IPCC, 2014). Future changes in shipping and other anthropogenic activities within the Arctic (Peters et al., 2011) can induce further climate change and health impacts in this sensitive region. The strong Arctic warming can also have far-reaching global implications (Zappa et al., 2018). For instance, there are signs that enhanced melting of Arctic sea ice and glaciers influences the Atlantic overturning circulation (Caesar et al., 2018; Yang et al., 2016). Cohen et al. (2014) and Coumou et al. (2018) point out that the AA can influence midlatitude weather via changes in storm tracks, the jet stream, and planetary waves and their associated energy propagation. Similarly, teleconnections between the Arctic and the Asian continent have been demonstrated through influences on the winter monsoon (Gong et al., 2001) and on the frequency of unusually hard winters (Kug et al., 2015) in East Asia.

Gregory Faluvegi, Matthew Kasoar, Alf Kirkevåg, Jean-François Lamarque, Dirk Olivié, Thomas Richardson, Maria Sand, Drew Shindell, Christopher J. Smith, Apostolos Voulgarakis

The AA is caused by local forcings and feedbacks as well as by remote forcing, but the relative importance of these impacts is still debated. While previous investigations commonly attributed the main cause of AA to the snow and ice albedo feedbacks (Hall, 2004; Manabe & Stouffer, 1980), an idealized model experiment by Alexeev et al. (2005), in which the surface albedo was fixed, demonstrated that poleward energy transport from lower latitudes alone could create an AA. The importance of lower-latitude impacts on the Arctic through transport of heat and moisture has been stressed by many studies (Graversen & Wang, 2009; Screen et al., 2012; Yoshimori et al., 2017), and a recent analysis by Yoshimori et al. (2017) found that the effect of remote forcing is predominant in the Arctic warming. Other studies report that the AA is dominated by local forcings and feedbacks (Stuecker et al., 2018) and point to the importance of processes such as the water vapor and cloud feedbacks (Graversen & Wang, 2009) or the lapse-rate and Planck feedbacks (Pithan & Mauritsen, 2014), in addition to the ice albedo feedback (Laîné et al., 2016; Screen & Simmonds, 2010). Whether or not local processes dominate, the possibility of an influence from forcing at lower latitudes remains. This makes the origin of this forcing relevant, as homogeneously distributed greenhouse gases and highly regional aerosols may influence the AA differently.

While several multimodel studies based on Coupled Model Intercomparison Project Phase 5 (CMIP5) models have focused on the Arctic (Barnes & Polvani, 2015; Clara & Dirk, 2017; Franzke et al., 2017; Huang et al., 2017), none have, to our knowledge, looked at different drivers independently. The Precipitation Driver Response Model Intercomparison Project (PDRMIP) (Myhre et al., 2017) provides a unique data set that allows for investigations into climate responses to separate and clearly defined climate drivers, such as greenhouse gases or aerosols, in a multimodel framework. This has led the way for several studies that have investigated various aspects of climate driver-response relationships from a global perspective (Liu et al., 2018; Samset et al., 2016; Samset et al., 2018; Stjern et al., 2017). Here we use the PDRMIP data set to analyze the climate response in the Arctic (defined as the region north of 60°N). Our main objective is to see whether clear differences exist with respect to how different climate drivers influence the Arctic. We do this by providing descriptive accounts of how changes to precipitation and the AA vary between the drivers. Our main focus is on experiments where the drivers are perturbed globally, but we also examine the response to isolated perturbations of aerosols in two different source regions. For aerosols and other short-lived climate drivers, the location of emissions can be important to the subsequent impact on global and regional climate (Lund et al., 2014; Sand et al., 2013; Sand et al., 2016; Screen et al., 2012; Shindell et al., 2008; Yang et al., 2018). Wobus et al. (2016) find that different future emission scenarios produce large variations in the resulting Arctic temperature change. Hence, as future changes in emissions and transport pathways (Jiao & Flanner, 2016) may shift the role of drivers, and their sources, in Arctic climate change, quantifying regional dependence of the forcing and response relationship is important. Combined, this will improve our understanding of the processes governing Arctic climate change today and allow us to make more informed predictions for future changes under various emission pathway scenarios.

The next section gives an account of the data and methodology used in the present analyses. Section 3 shows spatially and temporally resolved Arctic temperature responses to global perturbations of five climate drivers, including a quantification of the slow temperature-driven feedback response. A similar account of precipitation responses is given in section 4, including an energy budget analysis of differences between drivers. A separate analysis of Arctic responses to regional aerosol perturbations is presented in section 5. Results are discussed in section 6 and summarized in section 7.

2. Methods

The PDRMIP data set is described in detail by Myhre et al. (2017). Briefly, 10 global climate models performed experiments where five different climate drivers were perturbed separately. Relative to a baseline, the perturbations involved a doubling of CO_2 concentrations (CO2x2), a tripling of CH_4 concentrations (CH4x3), a 2% increase in the solar constant (SOL), a 10-fold increase in black carbon (BC) concentrations or emissions (BCx10), and a fivefold increase in SO_4 concentrations or emissions (SO4x5), respectively. In addition, seven of the models (see Table S1 in the supporting information) performed three regional experiments, which simulated the effects of a 10-fold increase in BC over Asia (BCx10asia) and in SO_4 over Asia and Europe (SO4x10asia and SO4x10europe). Here, Asia was defined as 10–50°N and 60–140°E and Europe as 35–70°N and 10–40°E. These results will be described in section 5.

All perturbations were instantaneous, and simulations were performed in two modes for both the baseline and perturbed states:

1. A fully coupled mode, for which equilibrium simulations were run for 100 years. Years 51–100 were used in our analyses. These simulations give the total climate response.
2. A setup with fixed sea surface temperatures (fixed-SST), which were run for 15 years. Years 6 to 15 were used in the analyses. These simulations give the fast (on the order of days to months) climate response.

The baseline represents present-day conditions focused at the beginning of this century (except HadGEM2-ES, which used preindustrial conditions), but the exact year and emission data set used varies slightly between models (see Table S1). For the aerosol experiments, five of the models (Table S1) performed concentration-driven simulations using identical aerosol concentrations based on the year 2000 monthly multimodel mean of the models in AeroCom Phase II (Myhre et al., 2013; Samset et al., 2013) as a baseline. Of the remaining models, one was not able to perform aerosol perturbations at all, while four used present-day aerosol emissions as a baseline. In the emission-driven models, responses to the increase in aerosols (e.g., increased precipitation) can feedback on the aerosol concentrations (e.g., increased wet removal of the aerosols) and potentially dampen or amplify the change. Sand et al. (2015) found in a comparison of emission-driven and concentration-driven BC perturbation experiments that Arctic responses were stronger in the emission-driven simulations. These model differences will therefore be kept in mind in the subsequent analyses.

The 10 models represent a selection of Earth system models with a broad variation in schemes and formulations. Three of the models include a representation of the radiative impact of BC on snow (Table S1). Furthermore, microphysical aerosol interactions with clouds (aerosol indirect effects) is accounted for in eight models (three of these also include an indirect effect of BC).

The fixed-SST simulations were utilized to calculate effective radiative forcing (ERF) as recommended in Forster et al. (2016), that is, the change in net radiative longwave (LW) plus shortwave (SW) fluxes at the top of atmosphere. As indicated above, the fixed-SST simulations are also used to study the fast (on the order of days to months) response of the climate system to the initial perturbation, also referred to as rapid adjustments. The total climate response, often (but not always) dominated by the surface-temperature change, is derived from the coupled simulations. These two sets of simulations then allow us also to extract the pure surface temperature-driven feedback response (also referred to as the slow response) as the total response minus the fast response.

3. Arctic Temperature Responses to Global perturbations

In this section, we document and discuss the Arctic temperature responses to the global perturbations. We cover annual mean and seasonally resolved surface responses, the separation between rapid responses and global surface temperature driven changes, and the vertical structure of the temperature response. We then conclude the section with a discussion on intermodel differences due to the inclusion of radiative effects of BC on snow in some of the models.

3.1. Annually and Seasonally Resolved Temperature Responses

As shown in previous PDRMIP studies (Myhre et al., 2017; Samset et al., 2016; Stjern et al., 2017), the different perturbations cause very dissimilar responses in global mean temperature and ERF, with model mean warming (and ERF) varying from 2.45 (3.78 W/m^2) for CO2x2 to 0.61 K (0.66 W/m^2) for BCx10. To facilitate comparison between the different climate drivers, Figure 1 shows changes per degree global temperature change in Arctic surface temperature (the AA) and precipitation for each given model and experiment. Hatched bars indicate the regional aerosol perturbation experiments, which will be discussed in section 5. For absolute changes for individual models, the reader is referred to Figure S1. Note here and throughout the paper that an increase in SO_4 gives a positive normalized temperature (and precipitation) change since the negative response it causes in the Arctic is normalized by a negative global temperature change. The horizontal grey line shows the average AA of the five global perturbations.

We find that the AA is not significantly different (at the 95 % confidence level, by using a Student's t-test) between any of the global experiments. The multi-model median AA ranges from 1.9 (SOL; ± an inter-

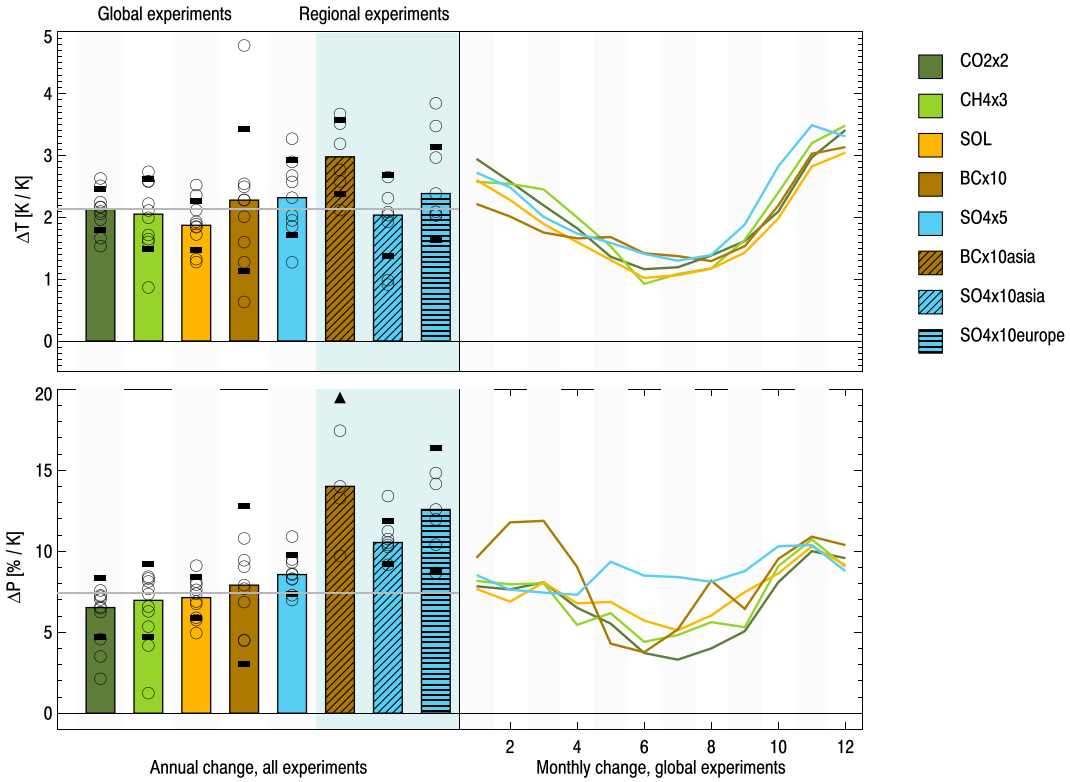

Figure 1. Responses in temperature and precipitation (normalized by the global mean temperature change) to perturbations in the five climate drivers, averaged over the Arctic (all area north of 60°N). Bars show annual model median values, and individual model values are shown as circles. The mean of the model-median values for the global cases is shown as a thick grey line. Horizontal bars indicate ± one standard deviation, and triangles are used to indicate when standard deviations are outside the range of the axes limits. Graphs show monthly mean changes (for the global experiments only).

model standard deviation of 0.4) to 2.3 (SO4x5; ± 0.6) between the drivers. The horizontal grey line shows the average AA of the five global perturbations, and none of the solid bars deviate much from this line. Note, however, that the inter-model spread is substantially larger than the differences in model median AA between experiments. This inter-model range is partly due to the large spread in Arctic responses, but also due to large model differences in the global response. For instance, the outlier in the upper panel of Figure 1 is CESM-CAM5, for which a very small global response to the BCx10 experiment produces an anomalously high AA. CESM-CAM5's weak temperature response is linked to the model's short BC lifetime for the BCx10 experiment (Stjern et al., 2017). With a few exceptions, we find that models with an above-average AA for one driver tend to have high values for all drivers (and vice versa). This means that the tendency of similar AA regardless of driver is found both for the multimodel medians and for individual models.

The AA is smallest during summer for all the climate drivers (Figure 1, upper rightmost panel). That amplification is weakest during Arctic summer is well documented elsewhere: in studies based on realistic historical or future scenarios with emission changes in both greenhouse gases and aerosols (Acosta Navarro et al., 2016; Laîné et al., 2016; Screen et al., 2012), in single-perturbation experiments of, for example, SO_4 (Yang et al., 2018) or CO_2 (Yoshimori et al., 2017), and in observations (Graversen et al., 2008). The positive ice albedo feedback is strongest in spring and summer but is counteracted by strong energy uptake by the Arctic ocean (Laîné et al., 2016), as well as by an increase in evaporation (Acosta Navarro et al., 2016; Laîné et al., 2016) and potentially also cloud responses (Crook et al., 2011; Yoshimori et al., 2017). During winter, conversely, the warming from heat release by the ocean is strengthened by positive cloud and lapse rate feedbacks (Laîné et al., 2016; Sejas et al., 2014). The dominating mechanisms contributing to this seasonal cycle differ between land and ocean surfaces, with the tendency for a stronger seasonal AA cycle over oceans (Laîné et al., 2016). Here we confirm that this seasonality is not a greenhouse gas-specific response but is in fact climate driver independent. To study the land/ocean contrast in seasonality, we have

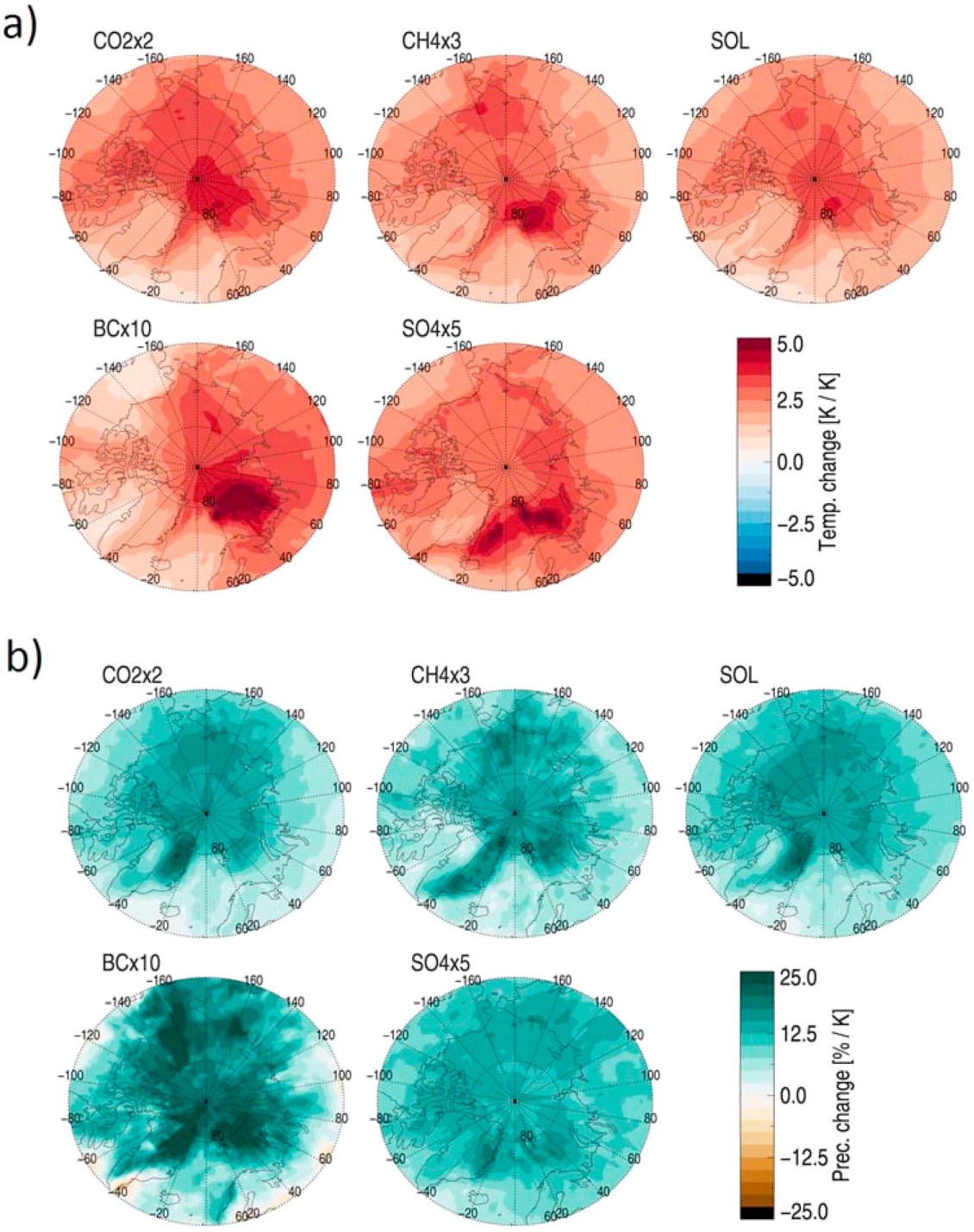

Figure 2. Multimodel median spatial patterns of (a) Arctic amplification and (b) precipitation changes normalized by global mean temperature change in the Arctic region, for each of the global experiments.

repeated the analysis behind Figure 1 for Arctic land-only and ocean-only responses. Figure S2 shows that the annually averaged AA is consistently stronger over ocean than over land, supporting Laîné et al. (2016). This is true for all drivers. We note that the land/ocean difference can partly be an effect of latitude: the higher Arctic (where AA is found to be stronger; see Figure 2) consists mostly of oceans while lower latitudes include much more land. Interestingly, over Arctic land surfaces, there seems to be a secondary maximum in spring/early summer for BCx10. This is potentially related to the inclusion of

the radiative effect of BC on snow (which is strongest in this season) in some models—see section 3.4 for further discussion.

3.2. Separating AA Into Rapid Responses and Feedbacks From Global Temperature Change

A key methodology in PDRMIP is to separate the climate response to an instantaneous perturbation into rapid responses (diagnosed from fixed sea-surface temperature simulations) and the slow feedback response to a change in global mean surface temperature. In Figure S3, we perform this separation for the AA shown in Figure 1.

Overall, we find weak rapid response contributions to AA. However, when removing the fast response to isolate the global mean temperature induced AA (the slow feedback response), the driver differences seen in Figure 1 are reduced (Figure S3). While the standard deviation of the multimodel median AA between the four warming Climate drivers (CO_2, CH_4, BC and SOL) is 0.16 for the total AA (Figure 1), the feedback response has a much smaller standard deviation of 0.03. SO_4, conversely, which had a not significantly stronger AA than the other drivers for the total response, has an AA feedback response that is 40% stronger than the other drivers, and the difference is now statistically significant.

The only driver to show a rapid adjustment AA significantly different from zero is CO_2. We interpret this to be due to its atmospheric absorption, which will act to heat the atmospheric column. The other driver with significant absorption, BC, has relatively little change in the Arctic, as discussed below.

Recently, Huneeus et al. (2014) compared climate effects of perturbations to CO_2 and the solar constant. They found that particularly for the feedback response, the similarity was remarkable, while rapid adjustments introduced more dissimilar responses. Overall, our results are consistent with this finding.

3.3. Geographical Temperature Response Patterns

In Figure 2, we show the multimodel geographical pattern of AA. Overall the different drivers produce qualitatively similar patterns, with a maximum around the northernmost parts of the Barents Sea, corresponding to the region where all climate drivers produce the greatest loss in sea ice (Figure S4). It should be noted that the location of this maximum warming may—at least partly—be an artifact of the tendency for models to have a low temperature bias in this region. For instance, Chapman and Walsh (2007) found that 12 out of 14 models have a cold temperature bias in the Barents Sea due to too extensive sea ice and that the same models showed strongest projected temperature changes in this region. Still, the main point—that warming patterns are similar between drivers—remains. Maps of ERF demonstrate that the radiative forcing for all drivers is larger at the lower latitudes than in the Arctic, meaning that the regional ERF pattern is not an important contribution to the AA (Figure 3). This is also true when we look at the pattern of ERF at the surface (not shown), which might be more indicative of regional responses than the top-of-atmosphere forcing. The similarity in AA patterns and the decoupling of the AA from the original forcing pattern further imply that the AA is not driver specific.

3.4. Vertical Structure of the AA

In Figure 4, we show the vertical structure of the AA. Some studies have suggested that the vertical dimension can provide further insights into the processes driving surface heating in the Arctic region. Sea ice or sea surface temperature changes are typically found to induce strongest response near the Arctic surface (Screen et al., 2012), while changes driven by processes such as changes in poleward heat transport or concentrations of water vapor or clouds will have a maximum response in the midtroposphere (Chung & Räisänen, 2011; Graversen & Wang, 2009; Yang et al., 2010). Note, however, that local responses and feedbacks will complicate such a clear interpretation.

As seen from Figure 4a, increases in CO_2, CH_4, the solar constant, and SO_4 cause very similar vertical patterns in the Arctic, with a strong surface AA and an upper-level (around 200 hPa) negative AA, visible as areas over Arctic latitudes with blue shades in the figure. This upper tropospheric cooling is a typical sign of a warming climate and an associated lifting of the tropopause, which causes temperatures to drop at pressure levels that used to be a part of the warmer stratosphere in the baseline simulations, but are included in the (colder) upper troposphere in the perturbed climate (see, e.g., Gillett et al., 2003). This is not to be confused with the well-known stratospheric cooling following increased CO_2 (Ramanathan & Dickinson, 1979), which is also visible in Figure 2a for CO2x2, but at higher altitudes. The upper tropospheric cooling is not

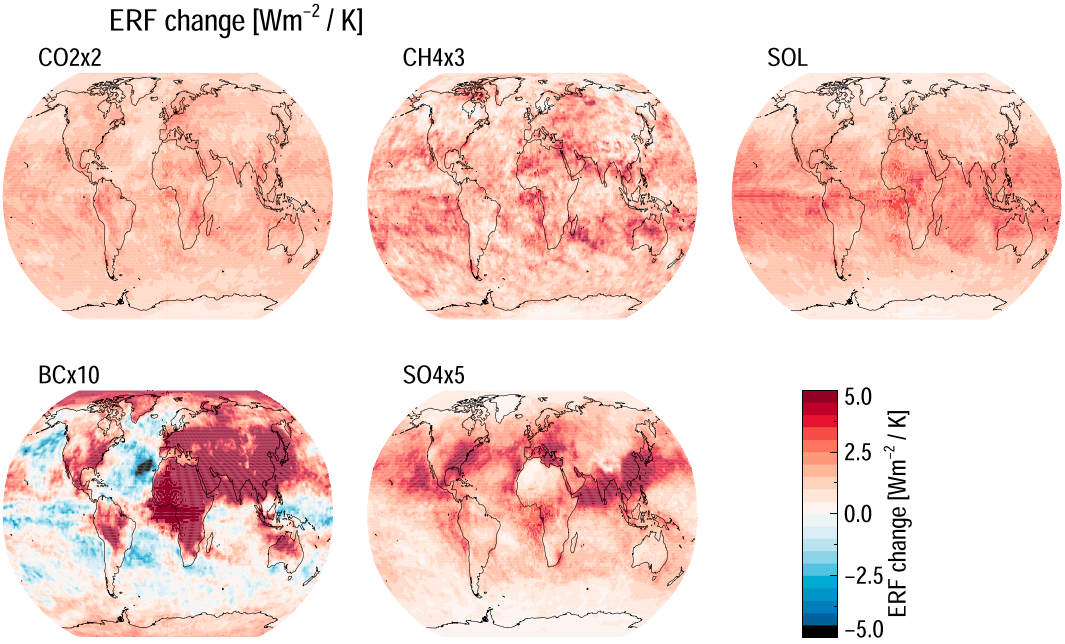

Figure 3. Multimodel median change in effective radiative forcing (ERF), normalized by the global mean temperature change, for the global experiments.

visible for BC in the annual mean, but in Figure 4b, where we show monthly mean Arctic changes, we find that BC causes a similar upper tropospheric cooling as the other climate drivers during January through March. For the rest of the year, however, the warming from BC extends throughout the atmospheric column. BC is known to induce efficient local heating of the atmosphere and has an absorption efficiency that increases with height (Samset & Myhre, 2011). In the Arctic, the atmospheric warming from BC absorption is particularly strong due to the high surface albedo. The warming pattern is therefore linked to the spatiotemporal distribution of BC concentrations. Figure S5a shows the BCx10 mass mixing ratio that the concentration-based models use as input. The largest BC concentration changes occur, as expected, at the surface around 40°N, where emissions are largest. At these latitudes, air masses are effectively lifted by convection, resulting in elevated concentrations also at higher altitudes, where aerosols are transported northward. This transport is most effective during summer and fall, as seen from the Arctic BC concentration changes in Figure S5b and the corresponding warming in Figure 4b. The strong decline in available SW radiation toward fall and winter also means that the radiative effect of increasing concentrations (i.e., absorption of SW and consequent atmospheric warming) will be highest in the summer. At lower altitudes, the polar dome limits the meridional transport into the Arctic, in particular during winter (Stohl, 2006). In addition, the aerosols that are lofted at lower latitudes give strong high-altitude warming, as illustrated in Figure S5c, where the seasonal warming averaged over East Asia, the major source region (Figure S5a), for the global BCx10 experiment is shown. This heat (and the associated increase in water vapor) therefore does not need to be elevated from the surface through convection but can be transported directly poleward.

Comparing the AA profile patterns between 0 and 90°N for winter and summer months separately (Figure S6, we find that the warming pattern for BCx10 has a much stronger poleward extension in summer, consistently with the strong within-Arctic summertime warming around 500 hPa. Graversen et al. (2008) found a similar upper-level summertime amplification in reanalysis data. They pointed out that the source of this high-altitude AA could not be surface driven (i.e., snow and ice feedbacks) and attributed it instead to summertime changes in the northward energy transport. This upper-level AA is however not visible in all reanalysis data sets (Bitz & Fu, 2008; Grant et al., 2008). While most pronounced for BC, the pattern of upper-level summertime warming is present for all climate drivers in our simulations. Dedicated studies are needed to further quantify the role of northward heat transport to the consistent heating around 500 hPa.

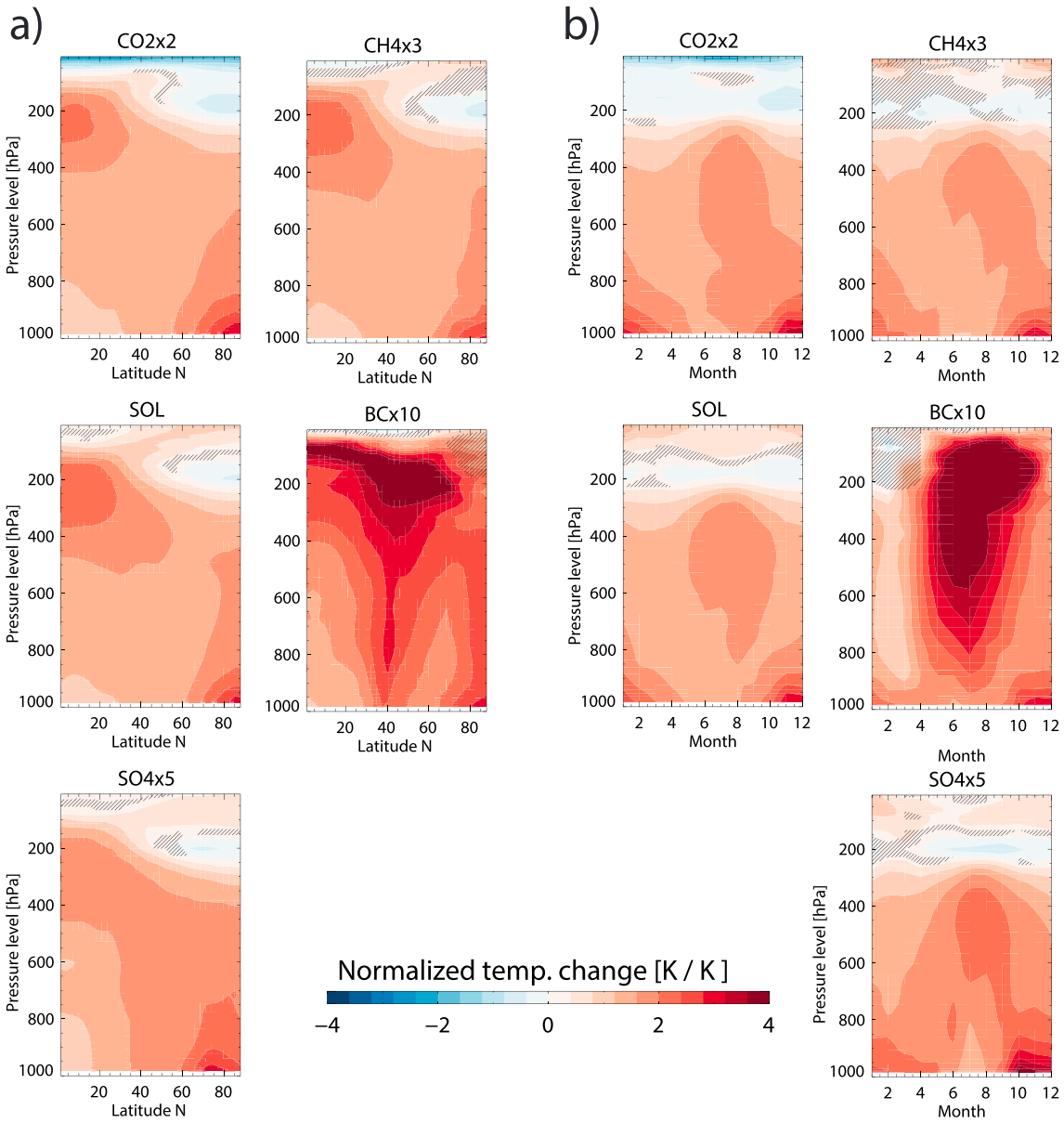

Figure 4. Multimodel median vertically resolved change in Arctic amplification for (a) the annual mean for latitudes 0 to 90°N and for (b) the Arctic (60 to 90°N) average for each month of the year. Hatching indicates where fewer than 75% of the models agree on the sign of the change.

For all drivers, the surface AA is lowest in summer. Previous studies have found that one reason for this is that (surface) warming from the ice albedo effect can be partially cancelled by an increase in summertime cloud cover (Crook et al., 2011). However, while an increase in summertime cloud cover is an expected response to the reduced sea ice cover in climate models (Vavrus, 2004; Yoshimori et al., 2014), observations indicate that the summer is the only season that lacks a cloud-response to sea ice changes (Morrison et al., 2018) and that the cloud response tends to be strongest in fall (Kay & Gettelman, 2009). Here we find that while the sea ice reductions are similar between the drivers (Figure S4), changes in cloud amounts vary (Figure 5), with no general tendency of a summertime increase for any of the drivers except BC. BCx10 causes a 5% increase in summertime low cloud cover (defined as the vertical average of cloud fractions between the surface and 680 hPa), contrasting a very weak increase or (for CO2x2) a reduction for the other climate drivers. The BC-induced increase in low level clouds would act both to dampen the summertime surface warming and (by reflecting incoming SW back toward the aerosol layer and adding to the amount of SW

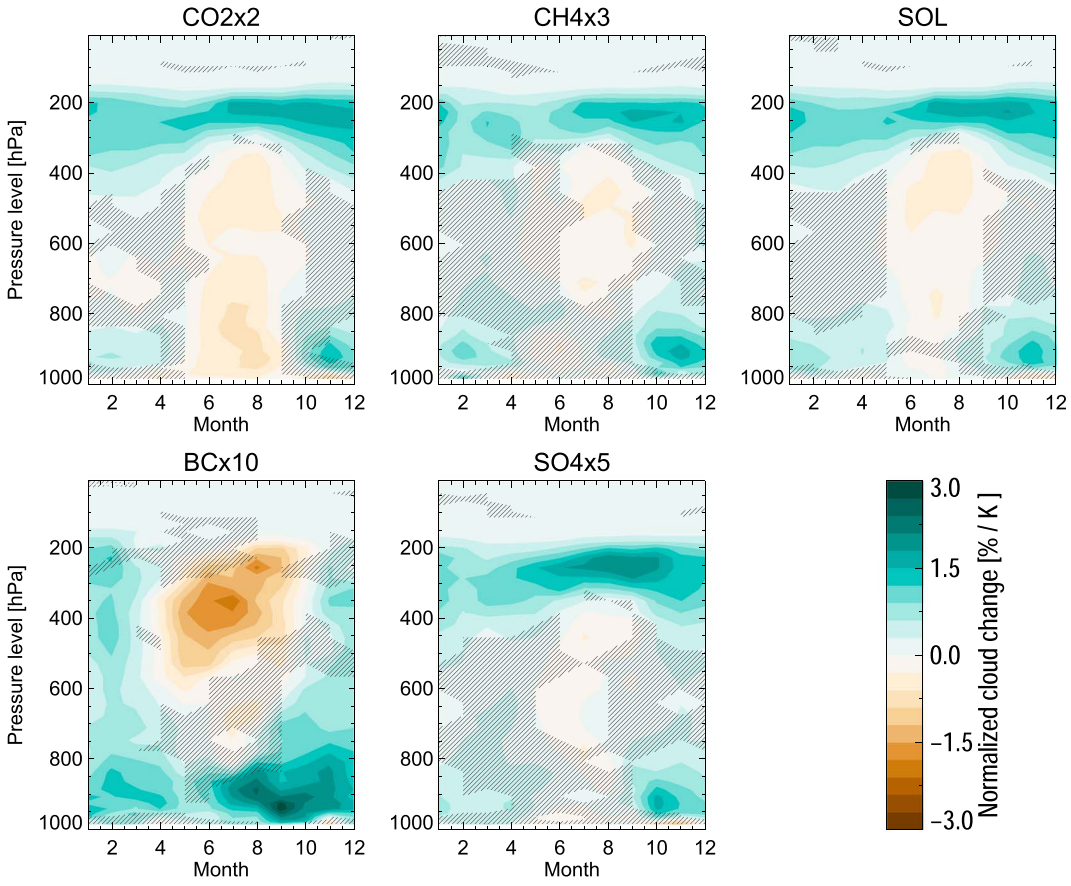

Figure 5. Multimodel mean vertically resolved cloud cover change (%) for the Arctic (60 to 90°N) average for each month of the year, normalized by global mean temperature change.

available for absorption) enhance the strong upper-level warming. Note also that around 500 hPa, all climate drivers cause a reduction in clouds, consistent with the upper-level summertime warming (Figure 4b). This response is strongest for BC, for which the warming is greatest.

In the wintertime, there is an upward shift of the lowermost clouds in response to all drivers, conceivably associated with an increase in specific humidity and therefore the lifting condensation level, as the atmosphere warms. A similar Arctic cloud response was found in a modeling study by Gillett et al. (2003) as a response to CO_2 doubling. Li et al. (2014) noted a link between reduced Arctic boundary layer stability and a deepening of the boundary layer in satellite data. The same features are found in our results during winter, seen as a thickening of the low-level cloud layer. This change in low-level wintertime cloud is important as it will primarily act to enhance the surface warming through their longwave warming effect in the absence of incoming solar radiation.

3.5. Model Differences in BC-Induced AA

Light-absorbing particles, such as BC, deposited on snow and ice may reduce the albedo and enhance melting, with potentially large impacts on the radiative budget. Of the 10 PDRMIP models, three include the radiative effect of BC on snow. Figure 6 shows AA responses to the BCx10 experiment from individual models. Model names are marked with [S] if they include BC on snow and are shown as solid lines in the right-hand panel. We focus on land-average AA, where BC snow-albedo effects are expected to be largest (Goldenson et al., 2012). Note that the CESM-CAM5 model has a particularly strong annual mean AA partly due to its very small global warming.

There does not seem to be a systematic difference in the seasonal AA cycle between the models with and without BC-on-snow treatment, except for a general tendency for higher AA in late fall/early winter. The

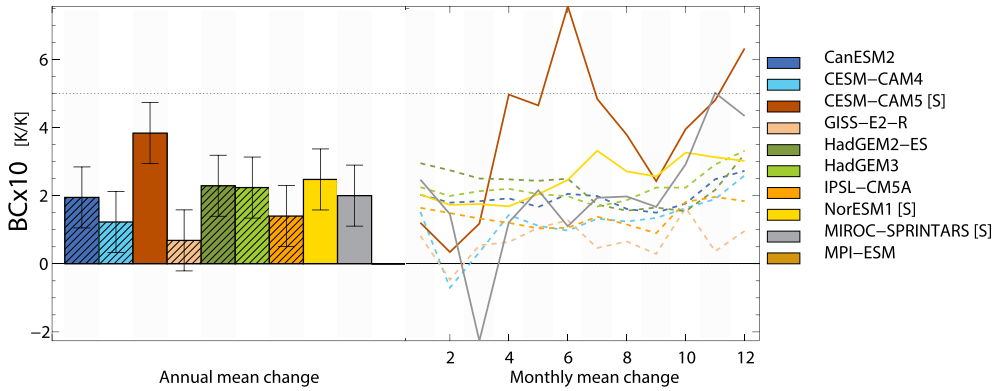

Figure 6. Annual mean (bars) and monthly mean (graphs) changes in land surface (normalized by global mean temperature change) Arctic amplification for the BCx10 experiment, for all contributing models. [S] indicates models with effect of black carbon (BC) on snow/ice. These are marked with solid lines, while dashed lines show models without the effect of BC on snow. See table S1 for futher model descriptions.

exception is CESM-CAM5, which has a very strong BC-induced amplification in spring/summer. This is consistent with Qian et al. (2014), who found that the Arctic forcing from BC on snow in the CAM5 model is substantial and is at its maximum around midsummer. There is a similar although weaker summertime maximum in NorESM1, but no such feature is discernible in MIROC-SPRINTARS. However, due to the wide variety of parameterizations and limited number of available models, these results should be interpreted with care. Further investigation of this effect requires a more dedicated study, where a larger number of models perform sensitivity studies with and without the effect of BC on snow.

4. Arctic Precipitation Responses to Global Perturbations

In this section, we discuss the Arctic precipitation response to the five global perturbations. As for temperature, we begin with the annual and seasonal mean responses and the impact of rapid adjustments. Then, we discuss precipitation change through the application of energy and moisture balance analyses.

4.1. Annually and Seasonally Resolved Precipitation Responses

While the Arctic surface temperature amplification has been thoroughly investigated, less attention has been given to changes in Arctic precipitation. Here we find that Arctic precipitation change per degree warming, often termed the apparent hydrological sensitivity, is similar (6–8%/K) for all the global perturbations (Figure 1). Samset et al. (2016) analyzed the globally averaged precipitation change for the PDRMIP data set and found a stronger apparent hydrological sensitivity for changes in aerosols and solar insolation (around 3%/K) than for greenhouse gas perturbations (around 2%/K). It was also found that the global average response to BCx10 was negative (i.e., a decrease). The Arctic hydrological sensitivity is thus found to be stronger than the global averages, consistent with previous findings from simulations using the RCP4.5 and RCP8.5 emission scenarios for a range of CMIP5 models (Bintanja & Selten, 2014). Here we are able to conclude that this is a robust feature among all drivers. Testing the 10 annual mean model values of SO_4-induced precipitation change against the other drivers using Student's ***t*** test, we find that SO_4 is associated with a slightly higher precipitation change, which is significantly (at the 95% level) different from the three other non-aerosol drivers.

As trends in Arctic precipitation follows the Arctic warming (Bintanja & Selten, 2014), the seasonal variation in the change generally resembles that of the AA, with a maximum in winter and smallest change during summer. Deser et al. (2010) performed idealized model experiments isolating the impact of future sea ice loss and found the same seasonality in sea ice and precipitation changes, indicating a close link. Our results also show the strongest precipitation changes coincident with the regions of strongest warming (Figure 2) and loss in sea ice (Figure S4), and we find that this also is where surface evaporation increases the most (not shown). The seasonal cycle in precipitation changes is most similar between the non-aerosol drivers (CO2x2, CH4x3, and SOL). For BCx10, the changes are stronger in late winter/spring than in November/December. For SO4x5 there is no clear summer minimum, and SO_4-induced precipitation

changes in April through October are the highest of all drivers. All drivers have a strong relative increase in summertime convective precipitation (not shown), particularly over land, except for BC, which causes a strong reduction due to increased stabilization connected with the strong upper-level warming shown in Figure 4b. However, the Arctic summertime precipitation is dominated by stratiform precipitation formation, so changes in convective clouds play a smaller role in the seasonal cycle of total precipitation. Instead, the seasonality can likely be attributed to seasonal variation in surface evaporation or moisture transport.

4.2. Separating Arctic Precipitation Amplification Into Rapid Responses and Feedbacks From Global Temperature Change

Like for temperature, we can separate the precipitation response into rapid adjustments and a slow change that scales with global mean surface temperature change, see Figure S3. Here the BC perturbation produces precipitation response in the Arctic of opposite sign from the global response (Samset et al., 2016; Stjern et al., 2017). Globally, the BC-induced drying has been shown to originate from the strong atmospheric absorption by the aerosols, which produces a very strong negative rapid adjustment that outweighs the final surface-temperature-driven increase (Andrews et al., 2010; Kvalevåg et al., 2013; Samset et al., 2016). However, Samset et al. (2016) demonstrated a regional dependency on the distribution between slow and fast changes, with a dominance of the slow response (increasing precipitation) in the Arctic region. This characteristic is confirmed in Figure S3, where the rapid precipitation response for BCx10 is close to zero.

4.3. Arctic Precipitation Changes Through an Energy Balance Perspective

To understand the mechanisms behind the Arctic precipitation changes for individual drivers, we utilize the energy budget approach (O'Gorman et al., 2011; Richardson et al., 2016). When we calculate the atmospheric energy budget, contributions to the total precipitation change can be subdivided into changes in longwave atmospheric cooling $\boldsymbol{LWC}$, shortwave atmospheric heating $\boldsymbol{SWH}$, the net upward sensible heat at the surface, $\boldsymbol{SH}$, and the dry static energy flux divergence $\boldsymbol{H}_{\mathrm{dry}}$:

$$\boldsymbol{LdP} = \boldsymbol{dLWC} - \boldsymbol{dSWH} - \boldsymbol{dSH} + \boldsymbol{dH_{dry}} \tag{1}$$

Above, $\boldsymbol{L}$ is the latent heat of condensation of water vapor and $\boldsymbol{P}$ is the surface precipitation. The column-integrated dry static energy flux divergence change $\mathrm{d}\boldsymbol{H}_{\mathrm{dry}}$ is calculated as the residual between the precipitation change $\boldsymbol{L}\mathrm{d}\boldsymbol{P}$ and the other terms and contributes positively to precipitation change if more dry static energy is transported out of the Arctic atmospheric column in the perturbed climate. Alternatively, we may use a simplified moisture budget, following Bintanja and Selten (2014):

$$\boldsymbol{LdP} = \boldsymbol{dE} + \boldsymbol{dF_{moisture}} \tag{2}$$

Here $\boldsymbol{E}$ denotes the evaporation from the surface, and the transport of moisture into the Arctic ($\mathrm{d}\boldsymbol{F}_{\mathrm{moisture}}$) is calculated as the difference between $\boldsymbol{L}\mathrm{d}\boldsymbol{P}$ and ds.

The energy and moisture budget analyses of total Arctic precipitation changes are shown in Figure 7a, again normalized by the global mean temperature change. Note that LdP indicates the total Arctic precipitation change per global warming, but in contrast to Figure 1, it shows model means (as opposed to model medians) and absolute changes (as opposed to relative changes). This is necessary to produce meaningful energy budgets and calculate residuals but gives rise to some differences between this figure and Figure 1. Immediately apparent from Figure 7a is how different the energy budget components are for the global BC perturbation compared to the other drivers. Even so, the total precipitation change is similar between BC and the other drivers, as in Figure 1.

Shortwave heating is shown with a negative prefix in Figure 7a, since a reduction in shortwave heating contributes to increased precipitation. For all drivers, this budget term is negative, indicating increases in shortwave atmospheric heating. In general, shortwave heating is driven by elevated atmospheric water vapor concentrations in the warmer climate (recall that the sign of the SO_4 responses are turned in the normalization by the global mean temperature change). However, due to the strong additional absorption by atmospheric BC particles, this term is by far strongest for BC. It is also stronger over land than over oceans (not shown) where BC concentrations are highest. Changes in longwave cooling are positive for all

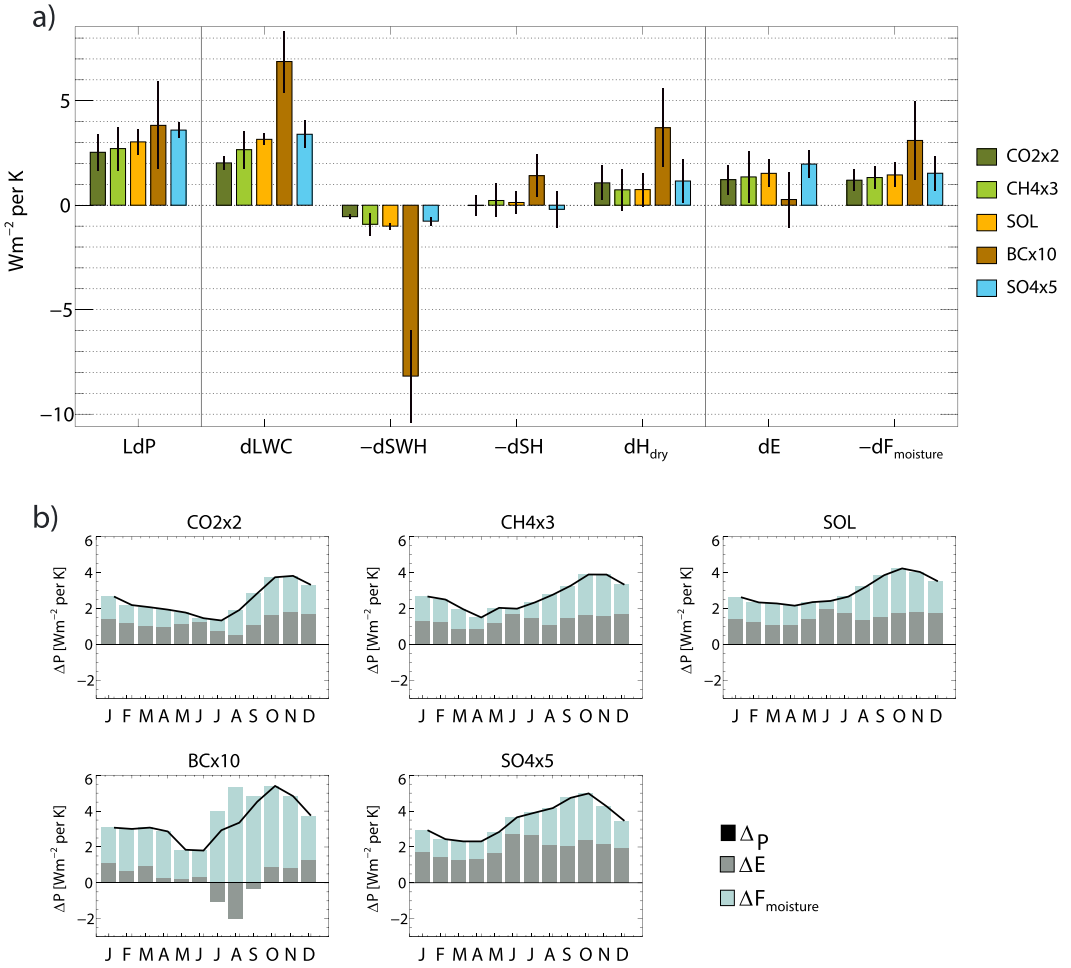

Figure 7. (a) Model mean atmospheric energy budget and moisture budget analysis for the Arctic, normalized by global mean temperature change. The sign convention is such that positive values indicate that the term contributes to increased precipitation. ***L***d***P*** is the total precipitation change. Components of the energy budget are shown in between the two vertical lines, where d***LWC*** is the change in longwave atmospheric cooling, d***SWH*** is the change in shortwave atmospheric heating, d***SH*** is the change in sensible heat at the surface, and d$\boldsymbol{H}_{\mathrm{dry}}$ is the change in dry static energy flux divergence. Components of the moisture budget are at the rightmost side, where d***E*** is change in surface evaporation and d$\boldsymbol{F}_{\mathrm{moisture}}$ is moisture transport into the Arctic. Vertical lines show the intermodel standard deviation. (b) Contribution of the moisture budget terms to the absolute monthly precipitation change.

drivers, again as a general response to the warming climate. The longwave cooling is strongest for BC since longwave radiation is re-emitted from high-altitude BC particles after their absorption of solar radiation. The smaller longwave cooling of CO2x2 than SO4x4 is because in the Arctic, as opposed to in the global average, the rapid response to an increase in CO_2 is a reduction in longwave cooling, which lowers its total increase. The sensible heat flux is affected by changes in the temperature difference between the surface and the overlaying air, as well as by changes in turbulence and convection. Globally, the change in this quantity is minor for all drivers but BC, as shown in a previous PDRMIP study (Myhre et al., 2018). We find that this is true also in the Arctic. The strong atmospheric warming caused by BC (Figure 4) leads to a marked reduction in the sensible heat flux, which is stronger over land than over oceans. Finally, all drivers cause an increase in the dry static energy flux divergence. This term is negative (indicating energy transport into the Arctic) in the baseline climate but slightly less negative in the perturbed climate, meaning that the poleward energy transport is reduced. This is a natural consequence of the AA, by which the high latitudes warm more than the lower latitudes and the meridional temperature gradient is reduced. For all drivers, but especially for BC, the reduced dry static energy flux divergence is strongest in the summer season (not shown).

Previous studies highlight the role of moisture transport from lower latitudes to Arctic precipitation changes (Bengtsson et al., 2011; Kug et al., 2010). Still, indications from both observations (Kattsov & Walsh, 2000) and model simulations (Bintanja & Selten, 2014) are that the dominating cause of the precipitation change may be the strong intensification of local surface evaporation. Here we find that the change in moisture transport ($d\boldsymbol{F}_{\text{moisture}}$) is of similar magnitude as increased evaporation ($d\boldsymbol{E}$) for CO2x2, CH4x3, and SOL. For SO_4, contribution from evaporation is higher than that from moisture transport, and for BC, there is a statistically significant higher impact from the latter, whereas the evaporation change is negligible. This means that the dominating processes behind Arctic precipitation changes may shift depending on what climate driver has the dominating impact in the Arctic.

We next examine the seasonal variations in the $d\boldsymbol{F}_{\text{moisture}}$ and $d\boldsymbol{E}$ terms and their contribution to the total precipitation change. In Figure 7b the seasonal absolute change in precipitation is shown as a solid black line, and the monthly contribution of evaporation and moisture transport changes to this precipitation change is indicated by the bars. For CO2x2, CH4x3, SOL, and SO4x5, the increase in surface evaporation is greatest in June, with a secondary maximum in late fall/early winter. BC, conversely, causes a small increase in evaporation in all seasons except summer, when there is a notable reduction. This is when available incoming solar radiation and enhanced BC concentrations combine to produce the seasonally strongest reduction in the amount of shortwave radiation that reaches the surface, an effect known as solar dimming. For BC, the moisture transport term is much larger than for the other drivers, and it is the dominant cause of the BC-induced Arctic precipitation changes. During winter, the relative importance of evaporation and moisture transport changes for SO_4 is comparable to the other (non-BC) drivers, while evaporation changes dominate in the summer. Recall, however, that the sign is turned by the normalization by a negative global mean temperature change. In reality, increased concentrations of SO_4 causes reduced moisture transport and evaporation throughout the year, but like for BC, there is a particularly strong reduction in evaporation in the summer months due to enhanced solar dimming. Conversely, CO_2 induces the weakest evaporation change of all the drivers in this season due to a negative rapid response (not shown) that lowers the total positive change. These differences explain the stronger precipitation response to SO_4 than to the other non-aerosol drivers, as shown in Figure 1.

For all drivers we find a maximum change in poleward moisture transport around August through October. This summer/autumn maximum is likely a contributing cause for the strong seasonal upper-level warming for BC, for which the moisture transport term is particularly strong. Moisture from lower latitudes can be a source of heat within the Arctic, in the form of latent heat release, increased water vapor greenhouse effect, or changes to clouds. Sedlar and Tjernström (2017) found a clear pattern of increased lower-level and decreased upper-level clouds in months with particularly strong moisture advection into the Arctic, similar to the cloud change pattern we see during summer for BCx10 (Figure 5).

We note for consistency that Bintanja and Selten (2014) found strongest late-century increases in moisture transport in summer/early autumn for a range of CMIP5 models under the RCP4.5 and RCP8.5 emission scenarios. The later seasonal maximum in our data is related to our broad definition of the Arctic as all area north of 60°N: using 70°N instead shifts the maximum transport change toward midsummer (see Figure S7).

5. Arctic Responses to Regional Perturbations

Seven of the 10 models performed additional simulations, where BC was perturbed in a subregion of Asia and SO_4 was perturbed in parts of Asia and Europe (see section 2 for detailed description of these regions). Two of these models ran emission-based simulations, leading to additional model differences due to differences in transport, wet removal, and other processes. The remaining five used concentration-based set-ups, which diminishes the sources for model differences and allows for more focus on dynamical responses. Given these differences, we have here chosen to present the concentration-based and the emission-based results separately, even if the latter will only show the mean of two models. Figure 8 shows the equivalent of Figure 1, where solid and hatched bars represent global and regional perturbations, respectively, but for the subset of five concentration-based models in Figure 8a and two emission-based in Figure 8b.

Starting with the concentration-driven models, we find that the Asian BC perturbation produces a stronger AA, as well as a stronger precipitation response, than the global perturbation. This contrasts the response to

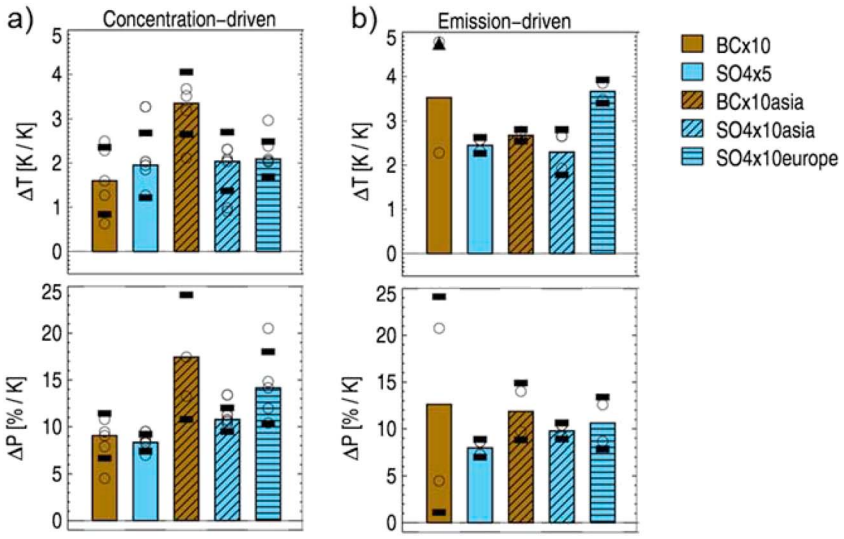

Figure 8. Responses in temperature and precipitation (normalized by the global mean temperature change) to global (solid bars) versus regional (hatched bars) perturbations in black carbon and SO_4, averaged over the Arctic, for (a) five concentration-based models (see Table S1) and (b) two emission-based models. Bars show annual model median values, and individual model values are shown as circles. Horizontal bars indicate ± one standard deviation, and triangles are used to indicate when standard deviations are outside the range of the axes limits.

the regional SO_4 perturbations, which both cause an AA more like the global experiment. There is a tendency for a stronger AA and stronger precipitation response from the European than from the Asian SO_4 perturbation, but the differences are not statistically significant. Figure 9a shows vertical AA profiles by latitude north, similar to Figure 4a, for the concentration-driven models. The warming pattern for

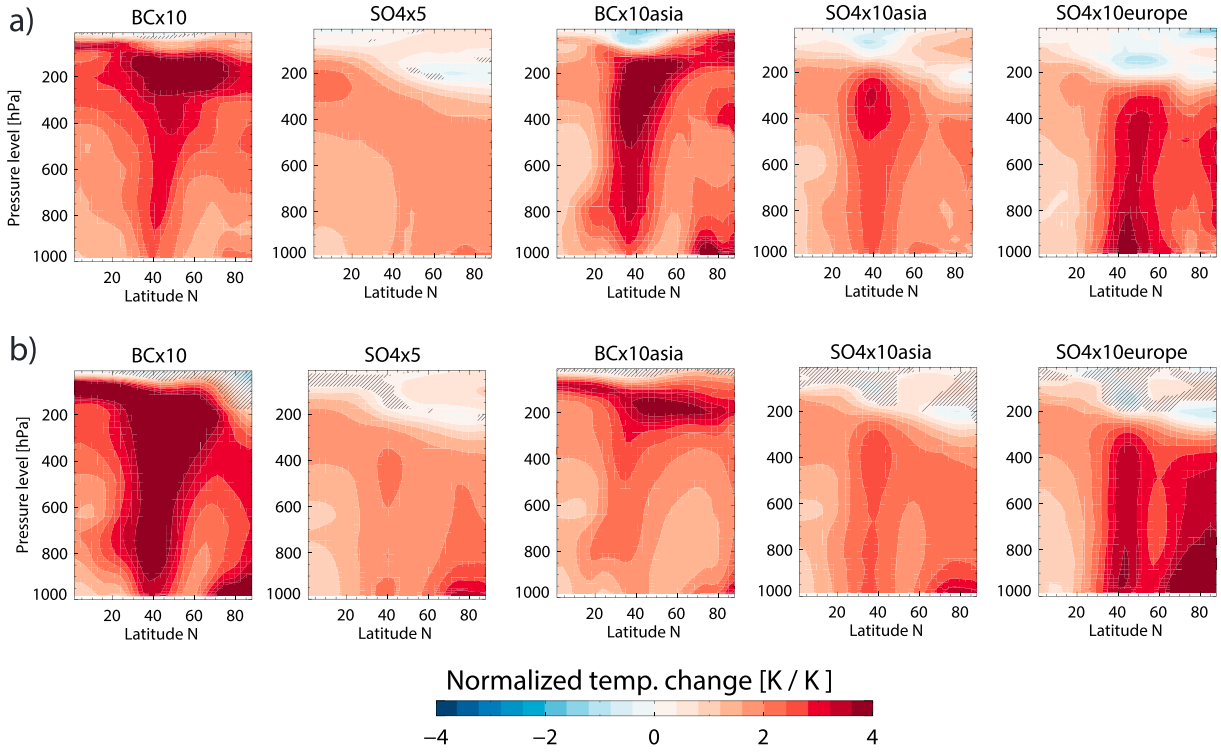

Figure 9. Multimodel median vertically resolved Arctic amplification for the annual mean for latitudes 0 to 90°N and for the model median on (a) five concentration-based models and (b) two emission-based models. Hatching indicates where fewer than 75% of the models agree on the sign of the change.

BCx10asia is more focused around the latitudes of the regional emissions (around 40°N) but otherwise resembles the global pattern. The AA signals from the regional SO_4 perturbations have much clearer maxima over the emission latitudes than the global signal, but as opposed to the regional BC perturbation, they do not show the same clear poleward extension of the AA.

The two emission-driven models (Figure 8b) have stronger AA than the concentration-driven models, both for the global and the regional experiments. As mentioned in section 2, emission-driven models have the potential for an amplified or dampened response since the model's climate response may feedback on the BC concentrations, as found in Sand et al. (2015). Notably, while regional BC perturbations caused stronger AA than global for the concentration-driven models, the opposite is true for the emission-driven, due to a very strong AA for the global perturbation. However, this includes results from NCAR-CAM5, which was seen to be an outlier (Figure 1). With the exception of the BCx10 experiment, the AA responses of the two individual emission-driven models are very similar (note the circles in the figure, indicating individual model values).

While the concentration-driven models had no discernible AA difference between the two regional SO_4 perturbations, the 10-fold increase in SO_4 in Europe causes a significantly stronger AA than a 10-fold increase in Asia for the emission-driven models. This difference is particularly clear in the summertime, while wintertime responses are more similar (not shown). The similarity in wintertime responses can be explained by that fact that during winter, Europe and Eurasia are both located within the polar dome (i.e., the surfaces of constant potential temperature). This, and the fact that parts of these regions are covered in snow in winter, which cools the near-surface air and eases transport into the polar dome, allows air masses from both these regions to reach the Arctic through low-level transport (Stohl, 2006). Air masses that are too warm (i.e., air originating from lower latitudes in summer) for isentropic transport reach the Arctic through lifting outside the polar dome and may subsequently slowly descend within. Indeed, comparing seasonal vertical warming patterns between the European and the Asian SO_4 perturbations in Figure S6, we see that while the summertime Arctic response to SO_4 perturbations in the (warmer, more remote, and with more effective convective lifting) Asian region is mostly confined to the midtroposphere, the impact from European SO_4 extends all the way to the surface. This produces notable differences in surface AA (Figure 8b) between the two experiments. A wintertime warming, conversely, is visible at the Arctic surface in both the European and the Asian SO_4 perturbation experiments. The Europe-only perturbation also yields a higher precipitation response than the Asian-only perturbation.

Our findings for the emission-driven models, that Arctic temperature and precipitation responses are significantly stronger for the European than for Asian perturbations, are in line with previous findings (Aamaas et al., 2016; Bellouin et al., 2016; Sand et al., 2016; Stjern et al., 2016; Yu et al., 2013). For instance, Sand et al. (2016) shows that Europe and Russia are the regions that influence Arctic temperatures the most per unit BC emissions, and the large sulfate emission change in Europe over the past decades have been linked to changes in Arctic sea ice cover (Acosta Navarro et al., 2016; Gagné et al., 2017; Mueller et al., 2018). The greater impact of European emissions is likely due to factors connected with the nearer proximity of Europe to the Arctic but may also be related to a saturation of aerosol-cloud interactions over East Asia, as well as a greater climatological cloud cover, which could mask the direct aerosol forcing in that region (Kasoar et al., 2018). In another PDRMIP analysis, Liu et al. (2018) also found that the forcing from European SO_4 increases had a stronger efficacy in terms of global temperatures and precipitation effects than that from the Asian region. In the present study, we find that the concentration-based models do not show this difference, at least in the Arctic. However, the regional PDRMIP simulations are limited in terms of number of regions, making it difficult to confidently conclude on regional impacts on Arctic climate.

6. Discussion

Common for the Arctic impact studies mentioned in the previous section is that they focus on responses per unit emissions. In reality, SO_2 emissions in Europe are relatively low today, while SO_2 emissions in India are currently increasing strongly (Li et al., 2017). Sand et al. (2016) stress that due to the large absolute emissions of Short-lived climate forcers (SLCF) (particularly BC) from the Asian continent, this is presently the largest source of SLCF-driven Arctic warming—both due to long-range transport and due to localized radiative impact and subsequent transport of heat and moisture. However, large emission changes in this region

are ongoing (van der A. et al., 2017). Recent studies suggest that emissions of sulfur dioxide in China have decreased by 75% over the past decade and that India is taking over as the largest single-region emitter (Li et al., 2017). In contrast, emissions of BC and CO_2 have continued to increase in both regions (e.g., Hoesly et al., 2017). Persad and Caldeira (2018) looked at impacts from anthropogenic aerosol (including both SO_4 and BC) changes in a range of regions, using the NCAR-CAM5 model, and found substantial variations in how emissions from different regions influence the global temperature. They found that regions that historically or presently account for the majority of anthropogenic aerosol emissions have the largest impacts on temperature, while regions where emissions currently have or are projected to have strong trends (i.e., India or East Africa) have smaller temperature impacts. This suggests that, globally averaged, the future distribution of main emission regions may have a smaller cooling potential than historically. Importantly, however, one reason for the small global temperature impact of Indian emissions was a regionally heterogeneous pattern of both positive and negative temperature responses. And while increased aerosol emissions in general cause a cooling, the Arctic response to Indian emission changes in this study was a warming.

Energy and moisture transport from lower latitudes play an important role in the impact on Arctic climate. Recent research has looked closer into how poleward energy transport contributes to current and future AA and to how it will react to the reduced meridional temperature gradient following an AA (Graversen, 2006; Jonas et al., 2016; Kapsch et al., 2013). They find that it is the transport of latent heat, and not of dry-static energy, that dominates the contribution to AA. As for future changes in these energy transport terms, simulations show that while models do not agree on the sign of the change in the total poleward heat transport, they all predict a reduction in the dry static energy transport (as the faster Arctic warming reduces the temperature gradient between high and low latitudes) and an increase in the latent heat transport (Hwang et al., 2011). Here we find that the contribution from the dry-static energy flux divergence to the Arctic precipitation change differs between climate drivers but is particularly important for BC. It is however positive for all drivers and all individual models, indicating a reduction in northward energy transport. We also find, for all drivers, an increase in the northward transport of moisture, consistent with Hwang et al. (2011). We note that the ocean has been shown to play an important role in the poleward heat transport (Nummelin et al., 2017), but here, we have not looked at changes in this component. A separate study investigating how different climate drivers influence the various elements of the poleward energy transport could improve our ability to predict how the Arctic would respond to future emission and climate changes.

Many of the processes involved when simulating climate responses in the Arctic are associated with high levels of uncertainty. One example is the effect of BC aerosols on ice and snow, with estimates ranging from relatively weak (Bond et al., 2013) to strong (Flanner et al., 2007) effects. Here three of the contributing models (NorESM1, CESM-CAM5, and MIROC-SPRINTARS) include estimates of the radiative effect of BC on snow in their models, but in only one of these (CESM-CAM5) do we see a clear signal from this effect in the seasonal warming in the Arctic. Differences in how models treat processes such as BC on snow nevertheless contribute to be a source of uncertainty and deviations between models. Previous multimodel studies have found that the spread in model responses is particularly large in the Arctic (Sand et al., 2017), and this is also the case here: Table S3 shows that the intermodel standard deviation for both temperature and precipitation is typically a factor three or more larger in the Arctic than globally.

7. Summary and Conclusion

The Arctic is influenced by both local and remote emissions (Acosta Navarro et al., 2016; Gagné et al., 2017). Presently, global and regional trends in emissions are shifting rapidly. While global CO_2 emissions are still increasing (Le Quéré et al., 2018), there are significant regional differences in air pollutant trends (Hoesly et al., 2017; Li et al., 2017). Combined with underlying climate change, potentially affecting transport pathways (Jiao & Flanner, 2016), this may shift the relative importance of individual climate drivers for Arctic climate change. Moreover, aerosol emissions in individual regions may have a different impact on Arctic climate to global perturbations.

The present study analyzes the response of perturbations to five individual climate drivers (CO_2, CH_4, the solar constant, SO_4, and BC), investigating effects on Arctic temperature and precipitation. While some notable differences exist, particularly for BC, response patterns in the vertical temperature profile are broadly similar between climate drivers. The AA in surface temperature ranges only from 1.9 [$\pm$0.4] (SOL) to 2.3

[±0.6] (SO4x5) between drivers, and interdriver differences are not statistically significant. As indicated in previous studies, the majority of the Arctic response seems to originate from a generalized dynamical response to the climate warming. This is also reflected in the present analysis through the similar surface AA pattern across all drivers and in the fact that all drivers cause the strongest surface warming in winter. All drivers display a similar pattern of upper-level (~400 hPa) AA in the summer and a reduction in cloud cover in the same altitude and season. For BC, we see a much stronger upper-level AA than for the other climate drivers. This is likely connected to increased high-level concentrations of BC in summer, as well as a very strong BC-induced summertime increase in poleward moisture transport, which may induce additional warming through shortwave absorption by BC particles and an added water vapor greenhouse effect. This warming does not propagate down to the Arctic surface. A stronger increase in summertime low cloud cover (which tends to cool the surface) for the BC perturbations may instead act as a buffering effect, so that all climate drivers end up causing relatively similar surface AA, with maxima in winter and minima in summer.

Global temperature change-normalized precipitation responses are also relatively similar between drivers, although less so than for temperature. SO_4 causes significantly stronger (normalized) precipitation increases than the other nonaerosol drivers, driven by a much stronger evaporation change. This difference is particularly pronounced in the summer. An energy budget breakdown of the contribution of different processes to the precipitation change shows that the BC response is substantially stronger than those of the other climate drivers in in all these processes. In total, however, the different contributions cancel out to leave a precipitation change similar to that from the other climate drivers. While changes in poleward moisture transport and changes in evaporation have similar contributions to the total precipitation change for CO2x2, CH4x3, and SOL, the aerosol-driven precipitation changes differ, with a dominance of moisture transport in the case of BCx10 and a dominance of evaporation changes for SO4x4.

Our study presents a first, comprehensive overview of how Arctic temperature and precipitation responds to individual climate drivers. While further analysis is needed to fully disentangle all the processes that act to shape the Arctic climate response, we conclude that overall, responses are similar enough to provide confidence in scenario-based projections for Arctic climate change regardless of the detailed balance between components of future emissions.

Acknowledgments
The PDRMIP model output is publicly available; for data access, visit http://www.cicero.uio.no/en/PDRMIP/PDRMIP-data-access. PDRMIP is partly funded through the Norwegian Research Council project NAPEX (project number 229778). O. B. acknowledges HPC resources from TGCC under the gencmip6 allocation provided by GENCI (Grand Equipement National de Calcul Intensif). Climate modeling at GISS is supported by the NASA Modeling, Analysis and Prediction program, and GISS simulations used resources provided by the NASA High-End Computing (HEC) Program through the NASA Center for Climate Simulation (NCCS) at Goddard Space Flight Center. T. T. was supported by the supercomputer system of the National Institute for Environmental Studies, Japan, the Environment Research and Technology Development Fund (S-12-3) of the Ministry of the Environment, Japan, and JSPS KAKENHI grants 15H01728 and 15K12190. D. O., A. K., and T. I. were supported by the Norwegian Research Council through the projects EVA (grant 229771), EarthClim (207711/E10), NOTUR (nn2345k), and NorStore (ns2345k). T. A. was supported by the Joint UK BEIS/Defra Met Office Hadley Centre Climate Programme (GA01101). M. K. and A. V. are supported by the Natural Environment Research Council under grant NE/K500872/1. Simulations with HadGEM3-GA4 were performed using the MONSooN system, a collaborative facility supplied under the Joint Weather and Climate Research Programme, which is a strategic partnership between the Met Office and the Natural Environment Research Council. T. R. and P. F. were supported by NERC grants NE/K007483/1 and NE/N006038/1.

References

Aamaas, B., Berntsen, T. K., Fuglestvedt, J. S., Shine, K. P., & Bellouin, N. (2016). Regional emission metrics for short-lived climate forcers from multiple models. *Atmospheric Chemistry and Physics*, *16*(11), 7451–7468. https://doi.org/10.5194/acp-16-7451-2016

Acosta Navarro, J. C., Varma, V., Riipinen, I., Seland, Ø., Kirkevåg, A., Struthers, H., et al. (2016). Amplification of Arctic warming by past air pollution reductions in Europe. *Nature Geoscience*, *9*, 277. https://doi.org/10.1038/ngeo2673

Alexeev, V. A., Langen, P. L., & Bates, J. R. (2005). Polar amplification of surface warming on an aquaplanet in "ghost forcing" experiments without sea ice feedbacks. *Climate Dynamics*, *24*(7), 655–666. https://doi.org/10.1007/s00382-005-0018-3

AMAP (2017), Snow, water, ice and permafrost in the Arctic (SWIPA), 2017*Rep*., xiv + 269 pp. pp, Oslo, Norway.

Andrews, T., Forster, P. M., Boucher, O., Bellouin, N., & Jones, A. (2010). Precipitation, radiative forcing and global temperature change. *Geophysical Research Letters*, *37*, L1470. https://doi.org/10.1029/2010GL043991

Anthony, K. W., Daanen, R., Anthony, P., Schneider von Deimling, T., Ping, C.-L., Chanton, J. P., & Grosse, G. (2016). Methane emissions proportional to permafrost carbon thawed in Arctic lakes since the 1950s. *Nature Geoscience*, *9*, 679. https://doi.org/10.1038/ngeo2795

Barnes, E. A., & Polvani, L. M. (2015). CMIP5 projections of Arctic amplification, of the North American/North Atlantic circulation, and of their relationship. *Journal of Climate*, *28*(13), 5254–5271. https://doi.org/10.1175/jcli-d-14-00589.1

Bellouin, N., Baker, L., Hodnebrog, Ø., Olivié, D., Cherian, R., Macintosh, C., et al. (2016). Regional and seasonal radiative forcing by perturbations to aerosol and ozone precursor emissions. *Atmospheric Chemistry and Physics*, *16*(21), 13,885–13,910. https://doi.org/10.5194/acp-16-13885-2016

Bengtsson, L., Hodges, K. I., Koumoutsaris, S., Zahn, M., & Keenlyside, N. (2011). The changing atmospheric water cycle in Polar Regions in a warmer climate. *Tellus A: Dynamic Meteorology and Oceanography*, *63*(5), 907–920. https://doi.org/10.1111/j.1600-0870.2011.00534.x

Bintanja, R., & Selten, F. M. (2014). Future increases in Arctic precipitation linked to local evaporation and sea-ice retreat. *Nature*, *509*, 479. https://doi.org/10.1038/nature13259

Bitz, C. M., & Fu, Q. (2008). Arctic warming aloft is data set dependent. *Nature*, *455*, E3. https://doi.org/10.1038/nature07258

Bond, T. C., Doherty, S. J., Fahey, D. W., Forster, P. M., Berntsen, T., DeAngelo, B. J., et al. (2013). Bounding the role of black carbon in the climate system: A scientific assessment. *Journal of Geophysical Research: Atmospheres*, *118*, 5380–5552. https://doi.org/10.1002/jgrd.50171

Caesar, L., Rahmstorf, S., Robinson, A., Feulner, G., & Saba, V. (2018). Observed fingerprint of a weakening Atlantic Ocean overturning circulation. *Nature*, *556*(7700), 191–196. https://doi.org/10.1038/s41586-018-0006-5

Chapman, W. L., & Walsh, J. E. (2007). Simulations of Arctic temperature and pressure by global coupled models. *Journal of Climate*, *20*(4), 609–632. https://doi.org/10.1175/jcli4026.1

Chung, C. E., & Räisänen, P. (2011). Origin of the Arctic warming in climate models. *Geophysical Research Letters*, *38*, L21704. https://doi.org/10.1029/2011GL049816

Clara, B., & Dirk, N. (2017). Drivers of Arctic Ocean warming in CMIP5 models. *Geophysical Research Letters*, *44*, 4263–4271. https://doi.org/10.1002/2016GL072342

Cohen, J., Screen, J. A., Furtado, J. C., Barlow, M., Whittleston, D., Coumou, D., et al. (2014). Recent Arctic amplification and extreme mid-latitude weather. *Nature Geoscience*, *7*(9), 627–637. https://doi.org/10.1038/ngeo2234

Coumou, D., Di Capua, G., Vavrus, S., Wang, L., & Wang, S. (2018). The influence of Arctic amplification on mid-latitude summer circulation. *Nature Communications*, *9*(1), 2959. https://doi.org/10.1038/s41467-018-05256-8

Cowtan, K., & Way, R. G. (2014). Coverage bias in the HadCRUT4 temperature series and its impact on recent temperature trends. *Quarterly Journal of the Royal Meteorological Society*, *140*(683), 1935–1944. https://doi.org/10.1002/qj.2297

Crook, J. A., Forster, P. M., & Stuber, N. (2011). Spatial patterns of modeled climate feedback and contributions to temperature response and polar amplification. *Journal of Climate*, *24*(14), 3575–3592. https://doi.org/10.1175/2011jcli3863.1

Deser, C., Tomas, R., Alexander, M., & Lawrence, D. (2010). The seasonal atmospheric response to projected Arctic sea ice loss in the late twenty-first century. *Journal of Climate*, *23*(2), 333–351. https://doi.org/10.1175/2009jcli3053.1

Flanner, M. G., Zender, C. S., Randerson, J. T., & Rasch, P. J. (2007). Present-day climate forcing and response from black carbon in snow. *Journal of Geophysical Research*, *112*, D11202. https://doi.org/10.1029/2006JD008003

Forster, P. M., Richardson, T., Maycock, A. C., Smith, C. J., Samset, B. H., Myhre, G., et al. (2016). Recommendations for diagnosing effective radiative forcing from climate models for CMIP6. *Journal of Geophysical Research: Atmospheres*, *121*, 12,460–12,475. https://doi.org/10.1002/2016JD025320

Franzke, C. L. E., Lee, S., & Feldstein, S. B. (2017). Evaluating Arctic warming mechanisms in CMIP5 models. *Climate Dynamics*, *48*(9), 3247–3260. https://doi.org/10.1007/s00382-016-3262-9

Gagné, M. È., Fyfe, J. C., Gillett, N. P., Polyakov, I. V., & Flato, G. M. (2017). Aerosol-driven increase in Arctic sea ice over the middle of the twentieth century. *Geophysical Research Letters*, *44*, 7338–7346. https://doi.org/10.1002/2016GL071941

Gillett, N. P., Allen, M. R., & Williams, K. D. (2003). Modelling the atmospheric response to doubled CO_2 and depleted stratospheric ozone using a stratosphere-resolving coupled GCM. *Quarterly Journal of the Royal Meteorological Society*, *129*(589), 947–966. https://doi.org/10.1256/qj.02.102

Goldenson, N., Doherty, S. J., Bitz, C. M., Holland, M. M., Light, B., & Conley, A. J. (2012). Arctic climate response to forcing from light-absorbing particles in snow and sea ice in CESM. *Atmospheric Chemistry and Physics*, *12*(17), 7903–7920. https://doi.org/10.5194/acp-12-7903-2012

Gong, D. Y., Wang, S. W., & Zhu, J. H. (2001). East Asian Winter Monsoon and Arctic Oscillation. *Geophysical Research Letters*, *28*(10), 2073–2076. https://doi.org/10.1029/2000GL012311

Grant, A. N., Brönnimann, S., & Haimberger, L. (2008). Recent Arctic warming vertical structure contested. *Nature*, *455*, E2. https://doi.org/10.1038/nature07257

Graversen, R. G. (2006). Do changes in the midlatitude circulation have any impact on the Arctic surface air temperature trend? *Journal of Climate*, *19*(20), 5422–5438. https://doi.org/10.1175/jcli3906.1

Graversen, R. G., Mauritsen, T., Tjernström, M., Källén, E., & Svensson, G. (2008). Vertical structure of recent Arctic warming. *Nature*, *451*, 53. https://doi.org/10.1038/nature06502

Graversen, R. G., & Wang, M. (2009). Polar amplification in a coupled climate model with locked albedo. *Climate Dynamics*, *33*(5), 629–643. https://doi.org/10.1007/s00382-009-0535-6

Hall, A. (2004). The Role of Surface Albedo Feedback in Climate. *Journal of Climate*, *17*(7), 1550–1568. https://doi.org/10.1175/1520-0442(2004)017<1550:Trosaf>2.0.Co;2

Hartmann, D. L., Tank, A. M. K., Rusticucci, M., Alexander, L. V., Brönnimann, S., Charabi, Y. A. R., et al. (2013). Observations: Atmosphere and surface. In T. F. Stocker, D. Qin, G.-K. Plattner, M. Tignor, S. K. Allen, J. Boschung, A. Nauels, Y. Xia, V. Bex, & P. M. Midgley (Eds.), *Climate change 2013: The physical science basis. Contribution of Working Group I to the Fifth Assessment Report of the Intergovernmental Panel on Climate Change*, (pp. 159–254). Cambridge, United Kingdom and New York, NY, USA: Cambridge University Press. https://doi.org/10.1017/CBO9781107415324.008

Hinzman, L. D., Deal, C. J., McGuire, A. D., Mernild, S. H., Polyakov, I. V., & Walsh, J. E. (2013). Trajectory of the Arctic as an integrated system. *Ecological Applications*, *23*(8), 1837–1868. https://doi.org/10.1890/11-1498.1

Hoesly, R. M., Smith, S. J., Feng, L., Klimont, Z., Janssens-Maenhout, G., Pitkanen, T., et al. (2017). Historical (1750–2014) anthropogenic emissions of reactive gases and aerosols from the Community Emission Data System (CEDS). *Geoscientific Model Development Discussion*, *2017*, 1–41. https://doi.org/10.5194/gmd-2017-43

Holland, M. M., & Bitz, C. M. (2003). Polar amplification of climate change in coupled models. *Climate Dynamics*, *21*(3), 221–232. https://doi.org/10.1007/s00382-003-0332-6

Huang, F., Zhou, X., & Wang, H. (2017). Arctic sea ice in CMIP5 climate model projections and their seasonal variability. *Acta Oceanologica Sinica*, *36*(8), 1–8. https://doi.org/10.1007/s13131-017-1029-8

Huneeus, N., Boucher, O., Alterskjaer, K., Cole, J. N. S., Curry, C. L., Ji, D., et al. (2014). Forcings and feedbacks in the GeoMIP ensemble for a reduction in solar irradiance and increase in CO_2. *Journal of Geophysical Research: Atmospheres*, *119*, 5226–5239. https://doi.org/10.1002/2013JD021110

Hwang, Y.-T., Frierson, D. M. W., & Kay, J. E. (2011). Coupling between Arctic feedbacks and changes in poleward energy transport. *Geophysical Research Letters*, *38*, L17704. https://doi.org/10.1029/2011GL048546

IPCC (2014). *Climate change 2014: Impacts, adaptation, and vulnerability. Part B: Regional aspects. Contribution of Working Group II to the Fifth Assessment Report of the Intergovernmental Panel on Climate Change*, 688 pp. Cambridge, United Kingdom and New York, NY, USA: Cambridge University Press.

Jiao, C., & Flanner, M. G. (2016). Changing black carbon transport to the Arctic from present day to the end of 21st century. *Journal of Geophysical Research: Atmospheres*, *121*, 4734–4750. https://doi.org/10.1002/2015JD023964

Jonas, M., Gunilla, S., G, G. R., Marie-Luise, K., C, S. J., & N, B. L. (2016). Melt onset over Arctic sea ice controlled by atmospheric moisture transport. *Geophysical Research Letters*, *43*, 6636–6642. https://doi.org/10.1002/2016GL069330

Kapsch, M.-L., Graversen, R. G., & Tjernström, M. (2013). Springtime atmospheric energy transport and the control of Arctic summer sea-ice extent. *Nature Climate Change*, *3*, 744. https://doi.org/10.1038/nclimate1884

Kasoar, M., Shawki, D., & Voulgarakis, A. (2018). Similar spatial patterns of global climate response to aerosols from different regions. *npj Climate and Atmospheric Science*, *1*(1), 12. https://doi.org/10.1038/s41612-018-0022-z

Kattsov, V. M., & Walsh, J. E. (2000). Twentieth-century trends of Arctic precipitation from observational data and a climate model simulation. *Journal of Climate*, *13*(8), 1362–1370. https://doi.org/10.1175/1520-0442(2000)013<1362:tctoap>2.0.co;2

Kay, J. E., & Gettelman, A. (2009). Cloud influence on and response to seasonal Arctic sea ice loss. *Journal of Geophysical Research*, *114*, D18204. https://doi.org/10.1029/2009JD011773

Kay, J. E., Holland, M. M., & Jahn, A. (2011). Inter-annual to multi-decadal Arctic sea ice extent trends in a warming world. *Geophysical Research Letters*, *38*, L15708. https://doi.org/10.1029/2011GL048008

Kug, J. S., Choi, D. H., Jin, F. F., Kwon, W. T., & Ren, H. L. (2010). Role of synoptic eddy feedback on polar climate responses to the anthropogenic forcing. *Geophysical Research Letters*, *37*, L14704. https://doi.org/10.1029/2010GL043673

Kug, J.-S., Jeong, J.-H., Jang, Y.-S., Kim, B.-M., Folland, C. K., Min, S.-K., & Son, S.-W. (2015). Two distinct influences of Arctic warming on cold winters over North America and East Asia. *Nature Geoscience*, *8*, 759. https://doi.org/10.1038/ngeo2517

Kvalevåg, M. M., Samset, B. H., & Myhre, G. (2013). Hydrological sensitivity to greenhouse gases and aerosols in a global climate model. *Geophysical Research Letters*, *40*, 1432–1438. https://doi.org/10.1002/grl.50318

Laîné, A., Yoshimori, M., & Abe-Ouchi, A. (2016). Surface Arctic amplification factors in CMIP5 models: Land and oceanic surfaces and seasonality. *Journal of Climate*, *29*(9), 3297–3316. https://doi.org/10.1175/jcli-d-15-0497.1

Le Quéré, C., Andrew, R. M., Friedlingstein, P., Sitch, S., Pongratz, J., Manning, A. C., et al. (2018). Global carbon budget 2017. *Earth System Science Data*, *10*(1), 405–448. https://doi.org/10.5194/essd-10-405-2018

Li, C., McLinden, C., Fioletov, V., Krotkov, N., Carn, S., Joiner, J., et al. (2017). India is overtaking China as the world's largest emitter of anthropogenic sulfur dioxide. *Scientific Reports*, *7*(1), 14304. https://doi.org/10.1038/s41598-017-14639-8

Li, Y., Thompson, D. W. J., Stephens, G. L., & Bony, S. (2014). A global survey of the instantaneous linkages between cloud vertical structure and large-scale climate. *Journal of Geophysical Research: Atmospheres*, *119*, 3770–3792. https://doi.org/10.1002/2013JD020669

Liu, L., Shawki, D., Voulgarakis, A., Kasoar, M., Samset, B. H., Myhre, G., et al. (2018). A PDRMIP Multimodel study on the impacts of regional aerosol forcings on global and regional precipitation. *Journal of Climate*, *31*(11), 4429–4447. https://doi.org/10.1175/jcli-d-17-0439.1

Lund, M. T., Berntsen, T. K., Heyes, C., Klimont, Z., & Samset, B. H. (2014). Global and regional climate impacts of black carbon and co-emitted species from the on-road diesel sector. *Atmospheric Environment*, *98*, 50–58. https://doi.org/10.1016/j.atmosenv.2014.08.033

Manabe, S., & Stouffer, R. J. (1980). Sensitivity of a global climate model to an increase of CO_2 concentration in the atmosphere. *Journal of Geophysical Research*, *85*(C10), 5529–5554. https://doi.org/10.1029/JC085iC10p05529

Morrison, A. L., Kay, J. E., Chepfer, H., Guzman, R., & Yettella, V. (2018). Isolating the liquid cloud response to recent Arctic sea ice variability using spaceborne lidar observations. *Journal of Geophysical Research: Atmospheres*, *123*, 473–490. https://doi.org/10.1002/2017JD027248

Mueller, B. L., Gillett, N. P., Monahan, A. H., & Zwiers, F. W. (2018). Attribution of Arctic sea ice decline from 1953 to 2012 to influences from natural, greenhouse gas, and anthropogenic aerosol forcing. *Journal of Climate*, *31*(19), 7771–7787. https://doi.org/10.1175/jcli-d-17-0552.1

Myhre, G., Forster, P. M., Samset, B. H., Hodnebrog, Ø., Sillmann, J., Aalbergsjø, S. G., et al. (2017). PDRMIP: A Precipitation Driver and Response Model Intercomparison Project, Protocol and preliminary results. *Bulletin of the American Meteorological Society*, *98*(6), 1185–1198. https://doi.org/10.1175/BAMS-D-16-0019.1

Myhre, G., Samset, B. H., Hodnebrog, Ø., Andrews, T., Boucher, O., Faluvegi, G., et al. (2018). Sensible heat has significantly affected the global hydrological cycle over the historical period. *Nature Communications*, *9*(1), 1922. https://doi.org/10.1038/s41467-018-04307-4

Myhre, G., Samset, B. H., Schulz, M., Balkanski, Y., Bauer, S., Berntsen, T. K., et al. (2013). Radiative forcing of the direct aerosol effect from AeroCom Phase II simulations. *Atmospheric Chemistry and Physics*, *13*(4), 1853–1877. https://doi.org/10.5194/acp-13-1853-2013

Notz, D., & Stroeve, J. (2016). Observed Arctic sea-ice loss directly follows anthropogenic CO_2 emission. *Science*, *354*(6313), 747–750. https://doi.org/10.1126/science.aag2345

Nummelin, A., Li, C., & Hezel, P. J. (2017). Connecting ocean heat transport changes from the midlatitudes to the Arctic Ocean. *Geophysical Research Letters*, *44*, 1899–1908. https://doi.org/10.1002/2016GL071333

O'Gorman, P. A., Allan, R. P., Byrne, M. P., & Previdi, M. (2011). Energetic constraints on precipitation under climate change. *Surveys in Geophysics*, *33*(3), 585–608. https://doi.org/10.1007/s10712-011-9159-6

Persad, G. G., & Caldeira, K. (2018). Divergent global-scale temperature effects from identical aerosols emitted in different regions. *Nature Communications*, *9*(1), 3289. https://doi.org/10.1038/s41467-018-05838-6

Peters, G. P., Nilssen, T. B., Lindholt, L., Eide, M. S., Glomsrød, S., Eide, L. I., & Fuglestvedt, J. S. (2011). Future emissions from shipping and petroleum activities in the Arctic. *Atmospheric Chemistry and Physics*, *11*(11), 5305–5320. https://doi.org/10.5194/acp-11-5305-2011

Pithan, F., & Mauritsen, T. (2014). Arctic amplification dominated by temperature feedbacks in contemporary climate models. *Nature Geoscience*, *7*, 181. https://doi.org/10.1038/ngeo2071

Qian, Y., Wang, H., Zhang, R., Flanner, M. G., & Rasch, P. J. (2014). A sensitivity study on modeling black carbon in snow and its radiative forcing over the Arctic and Northern China. *Environmental Research Letters*, *9*(6). https://doi.org/10.1088/1748-9326/9/6/064001

Ramanathan, V., & Dickinson, R. E. (1979). The role of stratospheric ozone in the zonal and seasonal radiative energy balance of the Earth-troposphere system. *Journal of the Atmospheric Sciences*, *36*(6), 1084–1104. https://doi.org/10.1175/1520-0469(1979)036<1084:tro-soi>2.0.co;2

Richardson, T. B., Samset, B. H., Andrews, T., Myhre, G., & Forster, P. M. (2016). An assessment of precipitation adjustment and feedback computation methods. *Journal of Geophysical Research: Atmospheres*, *121*, 11,608–11,619. https://doi.org/10.1002/2016JD025625

Samset, B. H., & Myhre, G. (2011). Vertical dependence of black carbon, sulphate and biomass burning aerosol radiative forcing. *Geophysical Research Letters*, *38*, L24802. https://doi.org/10.1029/2011GL049697

Samset, B. H., Myhre, G., Forster, P. M., Hodnebrog, Ø., Andrews, T., Boucher, O., et al. (2018). Weak hydrological sensitivity to temperature change over land, independent of climate forcing. *npj Climate and Atmospheric Science*, *1*(1), 20173. https://doi.org/10.1038/s41612-017-0005-5

Samset, B. H., Myhre, G., Forster, P. M., Hodnebrog, Ø., Andrews, T., Faluvegi, G., et al. (2016). Fast and slow precipitation responses to individual climate forcers: A PDRMIP multimodel study. *Geophysical Research Letters*, *43*, 2782–2791. https://doi.org/10.1002/2016GL068064

Samset, B. H., Myhre, G., Schulz, M., Balkanski, Y., Bauer, S., Berntsen, T. K., et al. (2013). Black carbon vertical profiles strongly affect its radiative forcing uncertainty. *Atmospheric Chemistry and Physics*, *13*(5), 2423–2434. https://doi.org/10.5194/acp-13-2423-2013

Sand, M., Berntsen, T. K., Seland, Ø., & Kristjánsson, J. E. (2013). Arctic surface temperature change to emissions of black carbon within Arctic or midlatitudes. *Journal of Geophysical Research: Atmospheres*, *118*, 7788–7798. https://doi.org/10.1002/jgrd.50613

Sand, M., Berntsen, T. K., von Salzen, K., Flanner, M. G., Langner, J., & Victor, D. G. (2016). Response of Arctic temperature to changes in emissions of short-lived climate forcers. *Nature Climate Change*, *6*(3), 286–289. https://doi.org/10.1038/nclimate2880

Sand, M., Iversen, T., Bohlinger, P., Kirkevåg, A., Seierstad, I., Seland, Ø., & Sorteberg, A. (2015). A standardized global climate model study showing unique properties for the climate response to black carbon aerosols. *Journal of Climate*, *28*(6), 2512–2526. https://doi.org/10.1175/jcli-d-14-00050.1

Sand, M., Samset, B. H., Balkanski, Y., Bauer, S., Bellouin, N., Berntsen, T. K., et al. (2017). Aerosols at the poles: An AeroCom phase II multi-model evaluation. *Atmospheric Chemistry and Physics*, *17*(19), 12,197–12,218. https://doi.org/10.5194/acp-17-12197-2017

Screen, J. A., Deser, C., & Simmonds, I. (2012). Local and remote controls on observed Arctic warming. *Geophysical Research Letters*, *39*, L10709. https://doi.org/10.1029/2012GL051598

Screen, J. A., & Simmonds, I. (2010). The central role of diminishing sea ice in recent Arctic temperature amplification. *Nature*, *464*, 1334. https://doi.org/10.1038/nature09051

Sedlar, J., & Tjernström, M. (2017). Clouds, warm air, and a climate cooling signal over the summer Arctic. *Geophysical Research Letters*, *44*, 1095–1103. https://doi.org/10.1002/2016GL071959

Sejas, S. A., Cai, M., Hu, A., Meehl, G. A., Washington, W., & Taylor, P. C. (2014). Individual feedback contributions to the seasonality of surface warming. *Journal of Climate*, *27*(14), 5653–5669. https://doi.org/10.1175/jcli-d-13-00658.1

Shepherd, A., Ivins, E. R., A, G., Barletta, V. R., Bentley, M. J., Bettadpur, S., et al. (2012). A reconciled estimate of ice-sheet mass balance. *Science*, *338*(6111), 1183–1189. https://doi.org/10.1126/science.1228102

Shindell, D. T., Chin, M., Dentener, F., Doherty, R. M., Faluvegi, G., Fiore, A. M., et al. (2008). A multi-model assessment of pollution transport to the Arctic. *Atmospheric Chemistry and Physics*, *8*(17), 5353–5372. https://doi.org/10.5194/acp-8-5353-2008

Stjern, C. W., Samset, B. H., Myhre, G., Bian, H., Chin, M., Davila, Y., et al. (2016). Global and regional radiative forcing from 20% reductions in BC, OC and SO4—An HTAP2 multi-model study. *Atmospheric Chemistry and Physics*, *16*(21), 13,579–13,599. https://doi.org/10.5194/acp-16-13579-2016

Stjern, C. W., Samset, B. H., Myhre, G., Forster, P. M., Hodnebrog, Ø., Andrews, T., et al. (2017). Rapid adjustments cause weak surface temperature response to increased black carbon concentrations. *Journal of Geophysical Research: Atmospheres*, *122*, 11,462–11,481. https://doi.org/10.1002/2017JD027326

Stohl, A. (2006). Characteristics of atmospheric transport into the Arctic troposphere. *Journal of Geophysical Research*, *111*, D11306. https://doi.org/10.1029/2005JD006888

Stuecker, M. F., Bitz, C. M., Armour, K. C., Proistosescu, C., Kang, S. M., Xie, S.-P., et al. (2018). Polar amplification dominated by local forcing and feedbacks. *Nature Climate Change*, *8*, 1076–1081. https://doi.org/10.1038/s41558-018-0339-y

van der A, R. J., Mijling, B., Ding, J., Koukouli, M. E., Liu, F., Li, Q., et al. (2017). Cleaning up the air: Effectiveness of air quality policy for SO_2 and NO_x emissions in China. *Atmospheric Chemistry and Physics*, *17*(3), 1775–1789. https://doi.org/10.5194/acp-17-1775-2017

Vavrus, S. (2004). The impact of cloud feedbacks on Arctic climate under greenhouse forcing. *Journal of Climate*, *17*(3), 603–615. https://doi.org/10.1175/1520-0442(2004)017<0603:tiocfo>2.0.co;2

Wobus, C., Flanner, M., Sarofim, M. C., Moura, M. C. P., & Smith, S. J. (2016). Future Arctic temperature change resulting from a range of aerosol emissions scenarios. *Earth's Future*, *4*(6), 270–281. https://doi.org/10.1002/2016EF000361

Yang, Q., Dixon, T. H., Myers, P. G., Bonin, J., Chambers, D., van den Broeke, M. R., et al. (2016). Recent increases in Arctic freshwater flux affects Labrador Sea convection and Atlantic overturning circulation. *Nature Communications*, *7*, 10525. https://doi.org/10.1038/ncomms10525

Yang, X. Y., Fyfe, J. C., & Flato, G. M. (2010). The role of poleward energy transport in Arctic temperature evolution. *Geophysical Research Letters*, *37*, L14803. https://doi.org/10.1029/2010GL043934

Yang, Y., Wang, H., Smith, S. J., Easter, R. C., & Rasch, P. J. (2018). Sulfate aerosol in the Arctic: Source attribution and radiative forcing. *Journal of Geophysical Research: Atmospheres*, *123*, 1899–1918. https://doi.org/10.1002/2017JD027298

Yoshimori, M., Abe-Ouchi, A., & Laîné, A. (2017). The role of atmospheric heat transport and regional feedbacks in the Arctic warming at equilibrium. *Climate Dynamics*, *49*(9), 3457–3472. https://doi.org/10.1007/s00382-017-3523-2

Yoshimori, M., Abe-Ouchi, A., Watanabe, M., Oka, A., & Ogura, T. (2014). Robust seasonality of Arctic warming processes in two different versions of the MIROC GCM. *Journal of Climate*, *27*(16), 6358–6375. https://doi.org/10.1175/jcli-d-14-00086.1

Yu, H., Chin, M., West, J. J., Atherton, C. S., Bellouin, N., Bergmann, D., et al. (2013). A multimodel assessment of the influence of regional anthropogenic emission reductions on aerosol direct radiative forcing and the role of intercontinental transport. *Journal of Geophysical Research: Atmospheres*, *118*, 700–720. https://doi.org/10.1029/2012JD018148

Zappa, G., Pithan, F., & Shepherd, T. G. (2018). Multimodel evidence for an atmospheric circulation response to Arctic sea ice loss in the CMIP5 future projections. *Geophysical Research Letters*, *45*, 1011–1019. https://doi.org/10.1002/2017GL076096